

Persistent Entropy as a Detector of Phase Transitions

Matteo Rucco - ruccomatteo@gmail.com

08/02/2026

Abstract

Persistent entropy (PE) is an information-theoretic summary statistic of persistence barcodes that has been widely used in numerical and experimental studies to detect regime changes in complex systems. Despite its empirical success, a general theoretical understanding of when and why persistent entropy reliably detects phase transitions has remained limited, particularly in settings where data and learned representations are inherently stochastic.

In this work, we establish a general, model-independent theorem providing sufficient conditions under which persistent entropy provably separates two phases. We formulate a probabilistic framework in which, for each system size N and control parameter λ , observational data define a random persistence diagram $D_N(\lambda)$ in a standard diagram metric space. Assuming (i) convergence in probability of persistence diagrams to deterministic limits on either side of a critical value λ_c , and (ii) a macroscopic feature separation condition—namely the presence of at least one persistent bar with lifetime bounded away from zero in one phase and only vanishingly short bars in the other—we show that persistent entropy exhibits an asymptotically non-vanishing gap across phases. The result relies only on continuity of PE along the convergent diagram sequence (or under mild regularization or lifetime truncation), and is therefore broadly applicable across data modalities, filtrations, and homological degrees.

To bridge asymptotic theory and finite-time computations, we introduce a dynamical operationalization based on topological stabilization: a topological transition time defined via the stabilization of a chosen topological statistic on a sliding window, and a probability-based estimator of critical parameters within a finite observation horizon. We validate the framework on three classes of systems: (i) the Kuramoto synchronization transition, (ii) the Vicsek order-disorder transition in collective motion, and (iii) neural network training dynamics across multiple datasets and architectures, where training loss acts as an effective control parameter. Across all experiments, stabilization of persistent entropy and collapse of variability across realizations provide robust numerical signatures of convergence toward low-complexity limiting persistence diagrams, in agreement with the theorem’s mechanism.

1 Introduction

Phase transitions are among the most fundamental phenomena in the study of complex systems, marking qualitative reorganizations of collective behavior induced by variations of control parameters. In classical statistical physics, phase transitions are traditionally characterized through the emergence or disappearance of local order parameters within the Landau symmetry-breaking paradigm. However, many contemporary systems of interest—including coupled oscillators, active matter, biological collectives, and data-driven dynamical models—exhibit high-dimensional, noisy, and heterogeneous dynamics for which suitable order parameters may be unknown, difficult to define, or strongly model-dependent. This has motivated the search for alternative, model-agnostic descriptors capable of capturing global structural changes associated with phase transitions.

Topology has emerged as a powerful framework for addressing this challenge. Unlike local observables, topological descriptors capture global geometric and connectivity properties that are invariant under continuous deformations. In condensed matter physics, topological phase transitions have fundamentally expanded the theory of critical phenomena beyond the Landau paradigm, replacing local order parameters with global topological invariants such as Chern numbers, winding numbers, and Berry phases. A vast body of work has demonstrated that such invariants undergo abrupt changes at critical points, leading to robust phenomena such as protected edge states and quantized transport, even in the absence of symmetry breaking [12, 36, 45]. More recently, topological ideas have been extended to dynamical, disordered, and driven systems, revealing universal mechanisms underlying phase transitions across a wide range of physical platforms [28, 15, 24].

Persistent homology, a central tool of topological data analysis [20, 9], provides a computationally tractable way to extract multiscale topological information from point clouds, networks, and time-dependent data. By encoding the birth and death of topological features across a filtration, persistent homology yields persistence diagrams or barcodes that summarize the global structure of data in a coordinate-free manner. Persistent homology has been successfully applied to detect regime changes and phase transitions in a variety of contexts, including synchronization dynamics [39, 46, 26], collective motion [43, 22], neural activity, and biological systems [33]. However, persistence diagrams are themselves high-dimensional objects, and their direct comparison is often computationally expensive and difficult to interpret.

Persistent entropy (PE) was introduced [13, 34, 35] as an information-theoretic scalar summary of persistence diagrams, designed to quantify their structural complexity in a stable and low-dimensional way. Empirically, persistent entropy has proven effective in detecting phase transitions and regime changes across a wide range of numerical and experimental studies [23, 46, 33]. Despite this growing body of applications, a fundamental theoretical question remains open: *under what general conditions does persistent entropy detect a phase transition, and what barcode-level mechanism underlies this detection?* At present, most uses of persistent entropy remain heuristic, relying on numerical evidence without a unifying theoretical explanation.

The aim of this work is to fill this gap. We provide a general, model-independent theorem establishing sufficient conditions under which persistent entropy provably detects a phase transition. Working within a probabilistic framework in which persistence diagrams are treated as random objects depending on system size, time, and control parameters [30, 10, 8], we show that whenever a phase transition induces a qualitative change in the limiting persistence diagrams—specifically, the appearance or disappearance of macroscopic persistent features—persistent entropy separates the phases by an asymptotically non-vanishing gap. The result relies on convergence in probability of persistence diagrams and on the continuity of persistent entropy [3] with respect to standard diagram metrics [14], and is therefore independent of the specific filtration, embedding, or data type considered.

Beyond establishing a static separation between phases, our framework naturally admits a dynamical interpretation. By tracking the time evolution of persistent entropy, we associate phase transitions with the stabilization of the underlying topological structure of the system. This leads to a time-resolved notion of topological transition, defined through the convergence of persistence diagrams and the stationarity of persistent entropy, and enables a probabilistic characterization of critical parameters in finite systems.

To complement the theoretical results, we introduce a numerical verification strategy based on finite-size scaling [23, 22] and probabilistic stability criteria, and we illustrate the theory using two paradigmatic models: the Kuramoto model of synchronization [41, 31] and the Vicsek model of collective motion [44, 42]. Despite their distinct microscopic dynamics and order parameters, both systems exhibit the same barcode-level mechanism at the transition, namely the disappearance of

macroscopic persistent features and the stabilization of persistent entropy. These results demonstrate that persistent entropy captures a universal topological signature of ordering transitions across different classes of dynamical systems.

Finally, we discuss broader implications of this framework for data-driven modeling and machine learning. Because persistent entropy provides a stable, low-dimensional summary of global topological structure [17, 18], it offers a principled way to incorporate physically meaningful inductive biases into learning algorithms and to monitor qualitative changes in learned representations during training. In this sense, the present work bridges topological data analysis, statistical physics, and machine learning, providing both a theoretical foundation and a practical methodology for entropy-based detection of phase transitions in complex systems.

2 Related work and state of the art

2.1 Persistent entropy

Topological data analysis (TDA), and persistent homology in particular, has emerged as a powerful framework for studying complex data arising from dynamical systems. Persistent homology provides a multiscale description of topological features and is equipped with strong stability guarantees under perturbations of the input. These properties have motivated its application to the detection of regime changes and phase transitions in a variety of systems, including synchronization phenomena, collective motion, and critical dynamics. In most cases, evidence that persistent homology detects phase transitions is empirical, relying on numerical experiments that show qualitative changes in persistence diagrams or summary statistics across parameter regimes. Persistent entropy (PE) was introduced as an information-theoretic summary of persistence barcodes, defined as the Shannon entropy of normalized persistence lifetimes. It provides a low-dimensional, noise-robust descriptor of topological complexity and has been successfully applied in many contexts, including time series analysis, biological systems, and networked dynamical systems. Its computational simplicity makes it particularly attractive for large-scale simulations and experimental data. Several studies have reported that PE varies sharply across phase transitions and correlates with classical order parameters, suggesting its potential role as a topological indicator of critical behavior.

Definition 1 (Persistent Entropy). *Let $D = \{(b_i, d_i)\}_{i=1}^m$ be a persistence diagram in a fixed homological degree, with finite lifetimes $\ell_i = d_i - b_i > 0$. Define the total lifetime*

$$L = \sum_{i=1}^m \ell_i.$$

If $m = 0$, we set $PE(D) = 0$. Otherwise, define probabilities

$$p_i = \frac{\ell_i}{L},$$

and the persistent entropy

$$PE(D) = - \sum_{i=1}^m p_i \log p_i.$$

This is the Shannon entropy of the normalized lifetime distribution. Variants such as normalized persistent entropy can be treated analogously.

Despite these promising results, the current literature largely treats persistent entropy as a heuristic or empirical diagnostic. While stability results guarantee robustness of PE under small perturbations of a fixed underlying object, they do not directly address situations in which the data-generating distribution itself changes with a control parameter, as is the case at phase transitions. As a result, there is currently no general theorem establishing when and why persistent entropy must detect a phase transition, even when persistent homology itself undergoes a qualitative change.

3 Research gaps and contributions

In many areas of physics, phase transitions are understood through changes in global or nonlocal properties rather than classical local order parameters. This is particularly evident in topological phases of matter, where phases are characterized by topological invariants and phase transitions correspond to changes in global structure. Recent developments emphasize critical behavior, universality, and scaling near topological transitions, extending beyond equilibrium band theory to interacting, driven, and disordered systems.[12, 36, 28, 45, 15, 25, 24]

Despite these advances, most existing approaches rely on model-specific constructions, symmetry assumptions, or analytically accessible observables. The present work addresses several open gaps at the intersection of phase transition theory and topological data analysis.

From phase transitions to persistence diagrams. While many dynamical systems are known to exhibit sharp transitions as a control parameter varies, there is no general theoretical framework linking such transitions to changes in persistence diagrams. In particular, existing results do not formalize when a phase transition induces the appearance or disappearance of macroscopic persistent features in the thermodynamic limit.[43, 39, 46, 23, 33, 26] This gap is especially evident in complex systems such as synchronization and active matter models, where topological signatures are observed numerically but lack rigorous justification.

Entropy-based summaries and rigor. Persistent entropy compresses the information contained in persistence diagrams into a single scalar quantity. Although widely used in applications, there is no general theorem explaining under which conditions a redistribution of persistence lifetimes across phases must lead to a non-vanishing entropy difference. [34, 17, 18, 35, 3, 29] Bridging this gap requires combining ideas from persistent homology, probability theory, and information theory.

Distributional convergence and finite-size effects. Most stability results in persistent homology concern perturbations of a fixed object. Phase transitions, however, involve changes in the underlying distribution of observed data as system size increases. A principled treatment therefore requires a probabilistic framework in which persistence diagrams are random objects and convergence is understood in a suitable metric sense. [22, 37, 10, 8, 30, 19] Such a framework is largely absent from the existing PE literature.

Persistent entropy and learning dynamics. Most existing uses of persistent entropy in machine learning treat it as a static or diagnostic summary computed from a fixed dataset, a trained model, or a short training snapshot [16]. However, learning dynamics fundamentally involve the evolution of a *distribution* over model parameters or representations induced by stochastic optimization, random initialization, and finite-sample effects [7, 27]. A principled understanding of

persistent entropy in this setting therefore requires a framework in which persistence diagrams associated with training trajectories are viewed as *random objects*, and their evolution is analyzed in terms of convergence in probability with respect to an appropriate diagram metric [2, 4]. Despite a growing body of empirical work employing persistent entropy for monitoring, feature augmentation, or post-hoc analysis [38, 16, 32], such a distributional and asymptotic perspective is largely absent from the machine-learning literature [11, 1]. As a consequence, it remains unclear when changes in persistent entropy during training reflect genuine structural convergence of learned representations, as opposed to finite-size fluctuations or optimization noise.

Contributions of this work. In this paper, we establish a general, model-independent theorem showing that persistent entropy detects phase transitions whenever the transition induces a qualitative separation in the *limiting distribution* of persistence diagrams. By treating persistence diagrams as random objects and formulating convergence in probability with respect to standard diagram metrics, our result identifies a minimal and verifiable mechanism. The mechanism aims to detect the appearance or disappearance of macroscopic persistent features under which persistent entropy separates phases with asymptotically non-vanishing probability. The theorem clarifies the role of embeddings and filtrations, isolates the precise regularity assumptions required for detection, and provides a principled link between finite-size observations and asymptotic behavior. Building on this framework, we introduce a dynamic finite-time criterion for identifying critical parameters and demonstrate its effectiveness across a range of physical systems (i.e., Kuramoto and Vicksek). We also present seminal numerical results to assess whether persistent entropy can improve understanding of neural network training dynamics. Taken together, these contributions place persistent entropy on a rigorous probabilistic footing and establish it as a theoretically justified tool for detecting emergent structural organization in complex, stochastic systems.

4 Phase transitions and persistence diagrams - Main theorem

4.1 Mathematical framework

We briefly clarify the mathematical setting used throughout the proof.

Random data and persistence diagrams. For each system size N and control parameter λ , the observed data (e.g. point clouds, weighted graphs, or embeddings constructed from dynamical trajectories) are random objects, due to randomness in initial conditions, intrinsic noise, or finite-size fluctuations. Applying a fixed filtration and a fixed homological degree k , we obtain a random persistence diagram $D_N(\lambda)$.

We view persistence diagrams as elements of the space \mathcal{D} of locally finite multisets of off-diagonal points in \mathbb{R}^2 , with the diagonal $\Delta = \{(t, t)\}$ included with infinite multiplicity. The space \mathcal{D} is endowed with a standard diagram metric, such as the bottleneck distance or a p -Wasserstein distance, defined via matchings that may pair off-diagonal points to the diagonal.

Convergence of persistence diagrams. Statements of the form

$$D_N(\lambda) \xrightarrow[N \rightarrow \infty]{\mathbb{P}} D(\lambda)$$

mean convergence in probability with respect to the chosen diagram metric d , that is, for every $\varepsilon > 0$,

$$\mathbb{P}(d(D_N(\lambda), D(\lambda)) > \varepsilon) \rightarrow 0 \quad \text{as } N \rightarrow \infty.$$

This expresses the concentration of the random persistence diagram around a deterministic limiting diagram as system size increases.

Persistent entropy as a random variable. Persistent entropy is a real-valued functional

$$PE : \mathcal{D} \longrightarrow \mathbb{R}_{\geq 0},$$

defined from the multiset of persistence lifetimes $\ell_i = d_i - b_i$ of the off-diagonal points in the diagram via normalized weights

$$p_i = \frac{\ell_i}{\sum_j \ell_j}, \quad PE(D) = - \sum_i p_i \log p_i,$$

whenever the total persistence $L = \sum_j \ell_j$ is finite and nonzero.

Persistent entropy is not uniformly continuous on the space of all persistence diagrams under the bottleneck distance, due to the possible creation or annihilation of many near-diagonal bars at arbitrarily small metric cost. However, it is continuous on subclasses of diagrams with uniformly controlled small-scale structure, for instance, diagrams with finite total persistence and negligible contribution from arbitrarily short bars, or under explicit lifetime truncation. Throughout, we assume that the random diagrams $D_N(\lambda)$ lie with high probability in such a class, so that convergence in probability of diagrams imply convergence in probability of persistent entropy.

Interpretation. Within this framework, phase transitions are detected by identifying qualitative changes in the limiting persistence diagram as the control parameter crosses a critical value. The theorem below formalizes the fact that, whenever such changes involve the appearance or disappearance of macroscopic persistent features, persistent entropy must reflect this transition.

4.2 Main theorem

Let $\lambda \in \mathbb{R}$ be a control parameter (e.g. coupling strength or noise level). For each system size N and parameter λ , assume we can construct a random persistence diagram $D_N(\lambda)$ from observational data (e.g. point clouds, weighted graphs, or embeddings) using a fixed filtration and a fixed homological degree k . Let λ_c be a critical value separating two phases.

Theorem 1 (Persistent entropy detects phase transitions). *Assume the following conditions hold.*

(A) **Diagram convergence.** *There exist deterministic persistence diagrams D_- and D_+ such that for every $\lambda < \lambda_c$,*

$$D_N(\lambda) \xrightarrow[N \rightarrow \infty]{\mathbb{P}} D_-,$$

and for every $\lambda > \lambda_c$,

$$D_N(\lambda) \xrightarrow[N \rightarrow \infty]{\mathbb{P}} D_+,$$

with respect to a standard diagram metric. Moreover, the diagrams $D_N(\lambda)$, D_- , and D_+ lie in a class on which persistent entropy is continuous, and both D_- and D_+ have finite total persistence.

(B) **Macroscopic feature separation.** *There exist constants $\delta > 0$ and $\varepsilon > 0$ such that:*

- *for $\lambda < \lambda_c$, the limiting diagram D_- contains at least one bar with lifetime at least δ ;*

- for $\lambda > \lambda_c$, all bars in D_+ have lifetimes at most ε .

Then for any $\lambda_- < \lambda_c < \lambda_+$, there exists a constant $\Delta > 0$ such that

$$\liminf_{N \rightarrow \infty} \mathbb{P}(PE(D_N(\lambda_-)) - PE(D_N(\lambda_+)) \geq \Delta) = 1.$$

In particular, persistent entropy separates the two phases with an asymptotically non-vanishing gap.

Proof. We treat the two phases separately.

Ordered phase ($\lambda > \lambda_c$). By assumption (B), all bars in the limiting diagram D_+ have lifetimes at most ε . Since D_+ has finite total persistence, its normalized lifetime distribution is concentrated on uniformly small weights. Consequently, the persistent entropy of D_+ is small; in the limiting case in which all lifetimes vanish one has $PE(D_+) = 0$, and more generally $PE(D_+) \leq c(\varepsilon)$ for some function $c(\varepsilon) \rightarrow 0$ as $\varepsilon \rightarrow 0$.

By assumption (A) and continuity of persistent entropy on the relevant class of diagrams,

$$PE(D_N(\lambda_+)) \xrightarrow[N \rightarrow \infty]{\mathbb{P}} PE(D_+).$$

Disordered phase ($\lambda < \lambda_c$). By assumption (B), the limiting diagram D_- contains at least one bar with lifetime $\ell_\star \geq \delta$. Let L_- denote the total persistence of D_- . The normalized weight of this bar satisfies

$$p_\star = \frac{\ell_\star}{L_-} \geq \frac{\delta}{L_-} > 0.$$

Therefore, the persistent entropy of D_- admits the positive lower bound

$$PE(D_-) \geq -p_\star \log p_\star > 0.$$

Again by assumption (A) and continuity of persistent entropy,

$$PE(D_N(\lambda_-)) \xrightarrow[N \rightarrow \infty]{\mathbb{P}} PE(D_-).$$

Conclusion. Combining the two limits, there exists $\Delta > 0$ such that, with probability tending to one as $N \rightarrow \infty$,

$$PE(D_N(\lambda_-)) - PE(D_N(\lambda_+)) \geq \Delta.$$

This proves that persistent entropy separates the two phases with an asymptotically non-vanishing gap. \square

Remark 1.

Metric structure. Persistence diagrams do not carry a natural inner-product structure; all arguments are formulated in the metric setting induced by standard diagram distances. The inclusion of the diagonal with infinite multiplicity is essential for the definition of these metrics.

Remark 2. Continuity of persistent entropy. Persistent entropy is not uniformly continuous on the space of all persistence diagrams under the bottleneck distance, due to the instability induced by arbitrarily many near-diagonal bars. The theorem relies only on continuity along the convergent sequence of diagrams, which is ensured under mild regularity assumptions or by explicit truncation of small lifetimes.

Remark 3. Mechanism of detection. The theorem shows that persistent entropy detects phase transitions whenever the transition induces or destroys a finite amount of topological mass at macroscopic scales. This identifies the barcode-level mechanism underlying the empirical success of persistent entropy in detecting regime changes in complex systems.

Remark 4. Model-independency. The theorem is model-independent. Detection depends on the choice of observable and filtration, but whenever a phase transition induces the appearance or disappearance of macroscopic persistent features, persistent entropy must detect it.

Corollary 1. If one phase admits at least one persistent topological feature with lifetime bounded away from zero and the other does not, persistent entropy acts as a consistent phase classifier.

5 Numerical experiments

5.1 Dynamic identification of the critical control parameter.

In finite-time numerical experiments, ordering transitions are observed as time-dependent relaxation processes: for a fixed control parameter λ , the system may or may not reach an ordered steady state within the observation horizon T_{\max} . To operationalize the theorem in this dynamical setting, we compute, for each λ and for each realization, a time series $S_\lambda(t)$ of a topological statistic derived from the persistence diagram $D_N(\lambda, t)$ (e.g., normalized persistent entropy $\text{NPE}(H_0)$ or the maximum H_1 lifetime). We then define the *topological transition time* $t_*(\lambda)$ as the earliest time at which $S_\lambda(t)$ becomes stable on a sliding window, namely

$$t_*(\lambda) = \min \left\{ t : \max_{s \in [t, t+W]} |S_\lambda(s) - S_\lambda(t)| \leq \varepsilon \right\},$$

where W is a fixed window length and ε is a tolerance capturing the numerical noise floor. Repeating this procedure over independent realizations yields an empirical probability of reaching topological stability within the observation horizon, $p(\lambda) = \Pr(t_*(\lambda) \leq T_{\max})$. Finally, the critical parameter is estimated by thresholding this probability: for example when applied to the Kuramoto model, we set $\hat{K}_c = \inf\{K : p(K) \geq p_0\}$, whereas for Vicsek (ordered at low noise) we set $\hat{\eta}_c = \sup\{\eta : p(\eta) \geq p_0\}$, with $p_0 \in (0, 1)$ a prescribed confidence level. This dynamic criterion is consistent with the theorem's mechanism, since stability of $S_\lambda(t)$ indicates convergence of $D_N(\lambda, t)$ toward a limiting, near-trivial diagram in the ordered phase.

Note that, in the following subsection, the Model \mathcal{M} is the Kuramoto model or the Vickse model and thus, λ is K or η accordingly.

5.2 The Kuramoto model

The Kuramoto model is widely used to model a network of limit-cycle oscillators that influence one another. The frequency of a single oscillator is influenced by its own intrinsic behavior and by the net pull of all the other oscillators. The reciprocal influences can be seen as the effect of a mean field that forces the oscillators to reach synchronization, i.e., to converge to the same phase. Mathematically, the model is a differential equation of the form:

$$\frac{d\theta_i}{dt} = \omega_i + \frac{K}{N} \sum_{j=1}^N G_{i,j} \sin(\theta_j - \theta_i)$$

where θ_i is the phase of the i -th oscillator with ω_i frequency. K is the coupling constant determining how much the intrinsic frequency can be modulated. $G_{i,j}$ is an adjacency matrix establishing the

Algorithm 1: Dynamic estimation of the critical control parameter via topological stability

Input: Model \mathcal{M} , parameter grid $\Lambda = \{\lambda_1, \dots, \lambda_m\}$, number of realizations R , observation horizon T_{\max} , sampling stride Δ , window length W , tolerance ε , confidence level p_0 .

Output: Estimated critical parameter $\hat{\lambda}_c$ and transition times $\{t_*^{(r)}(\lambda)\}$.

foreach $\lambda \in \Lambda$ **do**

for $r = 1$ **to** R **do**

Simulate \mathcal{M} at parameter λ and store states $X(\lambda, t)$ for $t \in [0, T_{\max}]$;

// Compute a time series of a topological statistic

Initialize an empty sequence $S_\lambda^{(r)}$;

for $t = 0, \Delta, 2\Delta, \dots, T_{\max}$ **do**

Build a distance matrix $d(\lambda, t)$ from $X(\lambda, t)$;

Compute persistence diagram $D_N(\lambda, t)$ (e.g., Vietoris–Rips);

Append statistic $S_\lambda^{(r)}(t) = \text{Stat}(D_N(\lambda, t))$ to $S_\lambda^{(r)}$;

// First time of stability on a sliding window

Set $t_*^{(r)}(\lambda) \leftarrow \min \left\{ t : \max_{s \in [t, t+W]} |S_\lambda^{(r)}(s) - S_\lambda^{(r)}(t)| \leq \varepsilon \right\}$;

If no such time exists, set $t_*^{(r)}(\lambda) \leftarrow \emptyset$;

Estimate $p(\lambda) = \frac{1}{R} \sum_{r=1}^R \mathbb{I}[t_*^{(r)}(\lambda) \leq T_{\max}]$;

if \mathcal{M} is Kuramoto **then**

$\hat{\lambda}_c \leftarrow \inf\{\lambda \in \Lambda : p(\lambda) \geq p_0\}$; // i.e., \hat{K}_c

else

$\hat{\lambda}_c \leftarrow \sup\{\lambda \in \Lambda : p(\lambda) \geq p_0\}$; // i.e., $\hat{\eta}_c$

return $\hat{\lambda}_c, \{t_*^{(r)}(\lambda)\}$;

connectivity among oscillators. In general, the system tends to converge in phase, which is the phase transition. A convenient measure of the *degree of synchronicity* is defined as follows:

$$r = \frac{1}{N} \sqrt{\left(\sum_{j=1}^N \cos(\theta_j) \right)^2 + \left(\sum_{j=1}^N \sin(\theta_j) \right)^2}$$

The degree r spans from zero to one; when $r = 1$ all the oscillators are in phase. Complete synchronization can be reached only for certain values of K that are greater than a critical value K_c . For a complete review of the Kuramoto model, we refer to [21].

Topological properties of the Kuramoto model were initially investigated in [40]. The authors used clique weight rank persistent homology (CWRPH[6]) for detecting relevant topological changes of the model between two different time regime $T_1 = [0, 250]$ and $T_2 = [250, 500]$. They used 128 oscillators connected through a given adjacency matrix $G_{i,j}$. At each simulation they selected the initial conditions, which are the frequency and the phase for each oscillator, and integrated the system between $t_0 = 0$ and $t_{\max} = 10$ with 500 time steps. The authors executed 20 simulations for each instance. At the end of all the simulations they built a function network by computing the *pairwise synchronicity coefficient* between two oscillators, defined as follows:

$$\phi_{i,j}^{T_k} = \langle |\cos(\theta_i^k - \theta_j^k)| \rangle$$

where $k = \{1, 2\}$ indicates the time regime and θ is the phase of the oscillator. The angular brackets refers to the average over the 20 simulations. The absolute value is imposed to simplify the interpretation of the coefficient. Since the networks are fully connected, their homology is trivial (i.e., only one connected component). Thus, the authors evaluated different thresholds for making the networks sparse. They highlighted the emergence of communities of oscillators and different topological structures between the two time regimes.

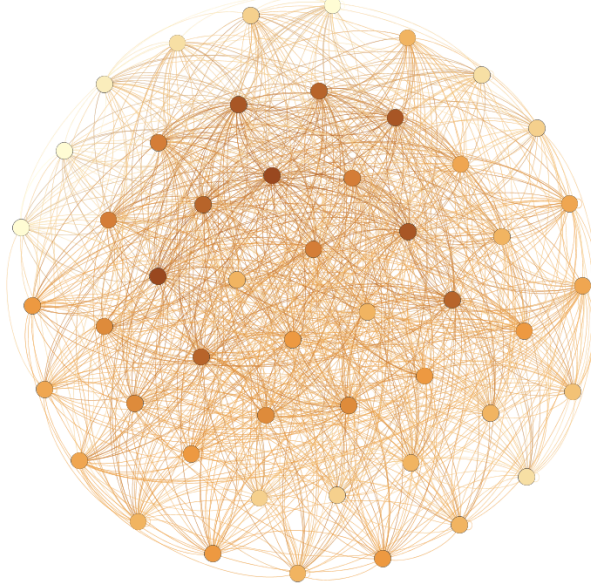


Figure 1: Kuramoto Network with 50 oscillators. The network layout is produced with the Fruchterman Reingold plugin of Gephi and the colour of each node is proportional to the degree [5]. The network is one example of the possible realizations.

5.2.1 Kuramoto model: experimental setup

Following the same lines of [40], we simulated different instances of the model. The instances differed by the adjacency matrix and the initial conditions, i.e., phase and frequency of each oscillator. The adjacency matrix was a random binary symmetric matrix without self-loops ($G_{i,i} = 0$). The initial frequencies were sampled from a Gaussian distribution with mean 0 and standard deviation 1, while the initial phases were sampled from a uniform distribution with values in $(0, 2\pi)$. We report here the results regarding the experiment with $N = 50$ oscillators. Network statistics are the following: number of nodes, 50; number of edges, 957; average degree, 38.28; density, 0.762. We integrated the Kuramoto models on 500 time points in the interval $T = [0, 10]$ ($\Delta t = 0.02$) for different values of the coupling coefficient $K \in [0.0, 16]$ with step 0.5. Each integration was repeated 10 times. The degree of synchronicity r as well as the pairwise synchronicity coefficient $\phi_{i,j}$ were computed for each K and for each time point.

5.2.2 Kuramoto model: experimental output analysis

Figure 2 summarizes the dynamical and figure 3 shows the topological behavior of the Kuramoto model across increasing values of the coupling strength K . For small coupling ($K = 0$ and $K = 1$),

the classical order parameter $r(t)$ remains low and fluctuating over time, indicating the absence of global synchronization. In this regime, the normalized persistent entropy $\text{NPE}(H_0)(t)$ exhibits sustained temporal variability and does not converge to a stable plateau, reflecting the persistent reconfiguration of connected components in the functional network induced by phase differences. Consistently, the corresponding persistence barcodes show a broad distribution of short-lived H_0 features and no stabilization in the filtration structure.

For small coupling values ($K = 0$ and $K = 1$), the Kuramoto system remains in an incoherent regime, as evidenced by the low and fluctuating values of the order parameter $r(t)$ in Fig. 2. In this regime, the normalized persistent entropy $\text{NPE}(H_0)(t)$ in Fig. 3 does not converge to a stable plateau, reflecting continuous rearrangements of the topological structure of the associated functional network. The corresponding persistence barcodes exhibit multiple short-lived H_0 features, with no dominant connected component (Fig. 4, top row).

As the coupling strength increases ($K = 3$), the system enters a transitional regime. Here, $r(t)$ grows gradually but remains subject to significant fluctuations, while $\text{NPE}(H_0)(t)$ displays enhanced temporal variability. This behavior indicates the coexistence of partially synchronized clusters and incoherent dynamics. Topologically, this regime is characterized by a progressive contraction of H_0 bar lifetimes without full stabilization, consistent with the presence of competing macroscopic configurations.

For larger coupling values ($K = 5$ and above), a qualitative transition is observed. The order parameter rapidly converges to $r(t) \simeq 1$ with negligible variance, signaling full synchronization. Concurrently, $\text{NPE}(H_0)(t)$ undergoes a sharp drop and stabilizes at a low constant value, indicating the collapse of topological complexity. This transition is directly visible in the persistence barcodes (Fig. 4, middle and bottom rows), where all but a single dominant H_0 feature vanish and higher homology groups are empty. For the representative realization at $K = 5$, the algorithm identifies a topological transition time $t_* \simeq 2.0$, after which the barcode structure remains unchanged.

This behavior is summarized quantitatively in Fig. 5, which reports the probability $\mathbb{P}(t_*(K) \leq T_{\max})$ of reaching topological stability within the observation horizon. The probability is close to zero in the incoherent regime, increases sharply in the transitional region, and saturates to one beyond the critical coupling \hat{K}_c . According to the dynamic criterion introduced in this work, \hat{K}_c marks the boundary beyond which synchronization is not only asymptotically stable but also dynamically accessible on finite time scales.

Overall, these results provide a coherent dynamical and topological characterization of the Kuramoto synchronization transition. In agreement with Theorem X, the phase transition corresponds to the emergence of convergence in probability of the persistence diagrams toward a near-trivial limiting structure, manifested numerically by the stabilization of persistent entropy and the collapse of macroscopic topological features.

5.2.3 Relation to the general theorem.

In the notation of Theorem 1, the control parameter is identified with the coupling strength $\lambda \equiv K$. For each system size N and each value of K , we construct a random persistence diagram $D_N(K, t)$ at time t by applying Vietoris–Rips persistent homology to the pairwise synchronicity matrix $\Phi(t) = (\phi_{i,j}(t))$, interpreted as a time-dependent distance matrix. The objective of the present numerical experiments is to verify, in the context of the Kuramoto model, the assumptions of Theorem 1, namely that the synchronization transition induces a qualitative separation in the limiting persistence diagrams, and that this separation is consistently detected by persistent entropy.

From the viewpoint of Theorem 1, the temporal evolution of persistent entropy can be interpreted as tracking the convergence of the time-dependent persistence diagrams $D_N(K, t)$ toward

the limiting diagram associated with the synchronized phase. In this framework, stationarity of persistent entropy corresponds to the stabilization of the underlying topological structure, indicating that the system has reached a steady state in which no macroscopic topological changes occur. Accordingly, we define a topological transition time $t_*(K)$ as the earliest time at which persistent entropy becomes stable within a prescribed tolerance over a sliding window.

The numerical results show that this topological criterion faithfully captures the dynamical behavior of the Kuramoto model. For small coupling values, persistent entropy exhibits sustained temporal fluctuations and does not reach a stable plateau, reflecting the persistence of incoherent phase configurations. As the coupling strength increases, a transitional regime emerges in which persistent entropy displays enhanced variability and intermittent stabilization, corresponding to the coexistence of partially synchronized clusters and incoherent dynamics. Beyond a critical coupling value \hat{K}_c , persistent entropy undergoes a sharp drop and rapidly stabilizes, indicating convergence of the persistence diagrams toward a near-trivial limiting structure.

This behavior is consistent with the classical synchronization transition observed through the Kuramoto order parameter, while highlighting a key distinction: persistent entropy is more sensitive to small phase rearrangements and thus provides an earlier and more granular signature of the approach to synchronization. In particular, synchronization in the Kuramoto model corresponds to the disappearance of persistent topological features whose lifetimes remain bounded away from zero as N increases, thereby realizing the macroscopic-bar separation assumed in Theorem 1. The resulting agreement between dynamical ordering, topological stabilization, and probabilistic convergence of persistence diagrams provides direct numerical support for the theoretical framework developed in this work.

5.3 The Vicsek model

The Vicsek model is a paradigmatic minimal model for collective motion in active matter, describing a system of N self-propelled particles moving in a two-dimensional domain with periodic boundary conditions. Each particle i is characterized by its position $\mathbf{r}_i(t) \in [0, L]^2$ and by a velocity of constant modulus v_0 with direction $\theta_i(t)$. The dynamics is defined by the discrete-time update rules

$$\theta_i(t + \Delta t) = \text{Arg} \left(\sum_{j: \|\mathbf{r}_j(t) - \mathbf{r}_i(t)\| < r} e^{i\theta_j(t)} \right) + \eta \xi_i(t), \quad (1)$$

$$\mathbf{r}_i(t + \Delta t) = \mathbf{r}_i(t) + v_0 \Delta t (\cos \theta_i(t), \sin \theta_i(t)), \quad (2)$$

where r is the interaction radius, η is the noise amplitude, and $\xi_i(t)$ are independent random variables uniformly distributed in $[-\frac{1}{2}, \frac{1}{2}]$. Distances are computed using periodic boundary conditions. For low noise or high density, the system undergoes a transition from a disordered phase to an ordered, flocking phase characterized by collective alignment of velocities.

A standard measure of collective order is the *polarization* defined as

$$\psi(t) = \frac{1}{N} \left\| \sum_{i=1}^N (\cos \theta_i(t), \sin \theta_i(t)) \right\| \in [0, 1]. \quad (3)$$

In the disordered phase $\psi(t) \approx 0$, while in the ordered phase $\psi(t)$ approaches 1, signaling global velocity alignment.

To characterize the topological structure of the Vicsek dynamics, we compute persistent homology from distance matrices derived from particle states. In particular, given a configuration at

time t , we consider either (i) a velocity-difference distance

$$d_{ij}^{(v)}(t) = \|\mathbf{v}_i(t) - \mathbf{v}_j(t)\|, \quad \mathbf{v}_i(t) = v_0(\cos \theta_i(t), \sin \theta_i(t)), \quad (4)$$

or (ii) an orientation-difference distance

$$d_{ij}^{(\theta)}(t) = 1 - |\cos(\theta_i(t) - \theta_j(t))|. \quad (5)$$

Both constructions yield symmetric distance matrices suitable for building Vietoris–Rips filtrations.

5.3.1 Vicksek model: experimental setup

To validate the proposed topological criterion on an active-matter system, we performed a numerical study of the Vicsek model across a range of noise amplitudes η . We considered a population of N self-propelled particles moving in a two-dimensional periodic square domain of side length L . Each particle i is characterized by its position $\mathbf{x}_i(t) \in [0, L]^2$ and orientation $\theta_i(t) \in [0, 2\pi)$, and moves at constant speed v_0 . At each discrete time step of size Δt , orientations are updated by aligning with the mean direction of neighboring particles within interaction radius r_{int} , perturbed by uniform angular noise of amplitude η , and positions are then advanced accordingly under periodic boundary conditions. In our implementation, for each value of η in a prescribed grid $\{\eta_1, \dots, \eta_m\}$ we generated R_η independent realizations by randomly sampling initial positions uniformly in the domain and initial orientations uniformly in $(0, 2\pi)$, and we simulated trajectories for T time steps.

For each realization and for a set of sampled times $t_k = k\Delta$ (with sampling stride Δ used to control computational cost), we computed a time-dependent distance matrix from the particle orientations and used it as input to Vietoris–Rips persistent homology. Specifically, letting $\theta_i(t_k)$ denote the orientation of particle i at time t_k , we constructed the pairwise orientation-difference distance

$$d_{ij}^{(\theta)}(t_k) = 1 - |\cos(\theta_i(t_k) - \theta_j(t_k))|,$$

(with the option to replace it by a velocity-based distance), and computed the normalized persistent entropy $\text{NPE}(H_0)(t_k)$ from the resulting persistence diagrams. To quantify the macroscopic ordering dynamics, we also evaluated the classical Vicsek polarization

$$\psi(t)$$

and reported mean curves with a shaded standard deviation band across realizations for both $\text{NPE}(H_0)(t)$ and $\psi(t)$. Finally, we applied the dynamic stability criterion introduced in this work by estimating, for each η , the topological transition time $t_*(\eta)$ as the first time at which $\text{NPE}(H_0)(t)$ becomes stable within a tolerance over a sliding window, and we used the empirical probability $\mathbb{P}(t_*(\eta) \leq T_{\text{max}})$ to identify the critical noise $\hat{\eta}_c$ separating noise levels for which topological stabilization (and thus flocking) is dynamically accessible within the observation horizon.

5.3.2 Vicksek model: experimental output analysis

Figure 6 shows the dynamical evolution of the Vicsek polarization $\psi(t)$ for increasing noise amplitudes. For small values of η (e.g., $\eta = 0.05$ and $\eta = 0.1$), the system rapidly develops global alignment and converges toward an ordered flocking state with $\psi(t) \simeq 1$ and minimal variability across realizations. As η increases, the convergence toward the ordered phase becomes slower and more heterogeneous, while for sufficiently large noise ($\eta = 0.5$) polarization remains strongly suppressed and fluctuating, indicating a disordered regime.

The corresponding topological evolution is captured by the temporal behavior of the normalized persistent entropy $\text{NPE}(H_0)(t)$ shown in Fig. 7. In the low-noise regime, persistent entropy decays rapidly, followed by clear stabilization, reflecting the collapse of topological complexity as particles align into a coherent flock. In contrast, for intermediate and high noise levels, $\text{NPE}(H_0)(t)$ exhibits sustained fluctuations and intermittent drops, indicating that the system explores multiple competing configurations without converging to a stable macroscopic structure.

This transition is further elucidated by the persistence barcodes in Fig. 8. At the initial time ($t = 0.0$), the H_0 barcodes display a wide distribution of lifetimes, corresponding to a highly fragmented configuration. At the algorithmically identified transition time $t_* \simeq 4.5$ for $\eta = 0.1$:contentReference[oaicite:1]index=1, the barcodes contract sharply, and a single dominant connected component emerges. At later times ($t = 9.5$), the barcode structure remains stable and trivial, with all higher-dimensional homology groups empty, confirming the persistence of the ordered phase.

The probabilistic summary of this behavior is reported in Fig. 9, which shows the probability $\mathbb{P}(t_*(\eta) \leq T_{\max})$ of reaching topological stability within the observation horizon. This probability is close to unity for small noise values and decreases as η increases, crossing the confidence threshold p_0 at a critical noise level $\hat{\eta}_c$. According to the dynamic criterion introduced in this work, $\hat{\eta}_c$ separates noise regimes for which the ordered phase is dynamically accessible on finite time scales from those in which it is not.

Taken together, these results demonstrate that the ordering transition in the Vicsek model admits a clear topological signature. In agreement with Theorem 1, the transition corresponds to the convergence in probability of the persistence diagrams toward a near-trivial limiting structure, manifested numerically by the stabilization of persistent entropy and the disappearance of macroscopic topological features.

5.3.3 Relation to the general theorem.

In the context of Theorem 1, the control parameter λ is identified with the noise amplitude η (or, equivalently, with other control parameters such as particle density or interaction radius). For each system size N and each value of η , we construct a time-dependent random persistence diagram $D_N(\eta, t)$ by applying Vietoris–Rips persistent homology to distance matrices derived from particle states. In the present study, these distances include both the velocity-difference metric $d_{ij}^{(v)}$ and the orientation-difference metric $d_{ij}^{(\theta)}$, thereby allowing us to assess the robustness of the topological signatures across different metric embeddings of the Vicsek dynamics.

The numerical experiments are designed to verify the assumptions of Theorem 1 for the Vicsek model in a fully dynamical setting. In the disordered phase, corresponding to large noise amplitudes η , particle orientations remain weakly correlated and the associated persistence diagrams exhibit only short-lived topological features. As a consequence, persistent entropy displays sustained temporal fluctuations and does not converge to a stable plateau within the observation horizon. In contrast, in the ordered flocking phase realized at small η , the emergence of coherent collective motion induces a rapid contraction of the persistence diagrams toward a near-trivial structure. This transition is characterized by the disappearance of topological features whose lifetimes remain bounded away from zero as N increases, thereby realizing the macroscopic-feature separation required by Theorem 1.

From the perspective of Theorem 1, the temporal evolution of persistent entropy provides a direct numerical proxy for the convergence in probability of the time-dependent persistence diagrams. The rapid decay and subsequent stabilization of $\text{NPE}(H_0)$ observed in the low-noise regime indicate that the system has reached a topologically stable ordered state, while the pronounced collapse of variance across realizations confirms that this convergence is robust and not driven by

finite-size or stochastic effects. By introducing a topological transition time $t_*(\eta)$ as the first time at which persistent entropy becomes stable, we further show that the Vicsek ordering transition can be characterized probabilistically through the quantity $\mathbb{P}(t_*(\eta) \leq T_{\max})$, leading to a well-defined estimate of the critical noise $\hat{\eta}_c$. Together, the orientation- and velocity-based analyses demonstrate that persistent entropy consistently detects the Vicsek order–disorder transition across different metric constructions, highlighting its robustness as a topological indicator of collective alignment dynamics.

5.4 Neural network training dynamics

We next consider the training dynamics of neural networks as a high-dimensional, non-physical system in which collective organization emerges in the space of parameters or learned representations. While no explicit spatial interactions are prescribed, stochastic gradient-based optimization induces an evolving geometry whose structure can be probed using topological methods.

We focus on supervised image classification tasks, where a neural network implements a parametric mapping

$$f_\theta : \mathcal{X} \rightarrow \mathcal{Y},$$

with parameters $\theta \in \mathbb{R}^P$ optimized by minimizing an empirical loss function

$$\mathcal{L}(\theta) = \frac{1}{|\mathcal{D}|} \sum_{(x,y) \in \mathcal{D}} \ell(f_\theta(x), y),$$

using stochastic gradient descent or adaptive variants. Training proceeds iteratively, producing a sequence of parameter values $\{\theta(t)\}_{t \geq 0}$, where t denotes the optimization step or epoch. Algorithm 2 summarizes the procedure used to compute persistent entropy from neural network training dynamics, treating training as a stochastic process and using metric embeddings of network parameters or representations to construct time-dependent persistence diagrams. Algorithm 2 was implemented as a Python notebook and executed on Google Colab; the code will be made publicly available.

Unlike classical physical models, neural network training does not admit a priori order parameters describing the internal organization of representations. Performance metrics such as accuracy provide only indirect information about the geometry induced by learning. Our goal is therefore to characterize the emergence of organized internal structure through topological observables derived from persistent homology.

5.4.1 Neural networks: experimental setup

We performed a systematic numerical study across multiple datasets and architectures, including DIGITS, MNIST, Fashion-MNIST, and CIFAR-10, using multilayer perceptrons (MLPs) and convolutional neural networks (CNNs). For each dataset, we considered architectures of increasing representational capacity and inductive bias. Fully connected models consisted of feedforward MLPs with one or two hidden layers (denoted MLP1 and MLP2), using ReLU nonlinearities and trained end-to-end on flattened input images. Convolutional models followed a standard CNN design with alternating convolutional and pooling layers, followed by one or more fully connected layers, thereby explicitly encoding spatial locality and weight sharing. Note that, for the DIGITS dataset, we restricted the analysis to fully connected architectures (MLP1 and MLP2) and did not include convolutional models. This choice is motivated by the low intrinsic complexity of the task: DIGITS images are low-dimensional, grayscale, and exhibit strong global structure with limited

spatial variability. In this regime, fully connected networks are already sufficient to achieve stable convergence and to induce a coherent internal representation geometry during training.

All networks were trained in a supervised classification setting using cross-entropy loss and stochastic gradient-based optimization. Training was performed for a fixed number of epochs, with identical hyperparameters across realizations within each dataset–architecture pair. To account for stochasticity in the training dynamics, we repeated each experiment over $R = 5$ independent runs, corresponding to different random initializations of network weights and different random seeds for data shuffling. This ensemble-based approach allowed us to treat training trajectories as realizations of an underlying stochastic process.

At each training epoch, we extracted weight-based representations by embedding hidden-layer neurons as points in a Euclidean space via their incoming weight vectors (including bias terms where applicable). Pairwise Euclidean distances between these vectors were used to construct distance matrices, which served as input to Vietoris–Rips filtrations. Persistent homology was then computed in homological degree H_1 , and the corresponding persistent entropy $\text{PE}(H_1)$ was evaluated as a low-dimensional summary statistic of the topological complexity of the parameter-space geometry.

In parallel, standard training observables such as the training loss were recorded. Rather than analyzing persistent entropy as a function of epoch index, we treated the training loss as an effective control parameter and aggregated results by binning loss values across realizations. This loss-based parametrization enables direct comparison between runs with different convergence speeds and provides a natural ordering of training stages in terms of optimization progress. For each bin, mean persistent entropy curves and 95% confidence intervals were computed, yielding the comparative plots summarized in Fig. 10.

5.4.2 Neural networks: experimental output analysis

Neural networks: DIGITS We begin with the DIGITS dataset, which represents a low-complexity supervised learning task characterized by low-dimensional inputs and limited intra-class variability. In this regime, stable internal representations are expected to emerge robustly during training, providing a favorable setting for the appearance of a limiting topological structure.

The DIGITS results are shown in the leftmost column of Fig. 10. For the shallow architecture (MLP1, top row), persistent entropy exhibits a clear and monotone decay as the training loss decreases, together with a rapid reduction in variability across realizations. This behavior indicates convergence toward a stable low-complexity topology in parameter space, reflecting the emergence of an organized solution manifold during training.

A similar but even more pronounced trend is observed for the deeper architecture (MLP2, middle row). As shown in Fig. 10, persistent entropy decreases smoothly across the full range of training loss values and exhibits minimal variability in the low-loss regime, indicating particularly robust convergence of the associated persistence diagrams. These results confirm that, for low-complexity tasks, convergence toward a stable topological structure occurs generically across architectures.

Neural networks: MNIST We next consider the MNIST dataset, which represents a canonical intermediate-complexity benchmark between DIGITS and Fashion-MNIST. While MNIST images are higher-dimensional than DIGITS, they retain strong low-level regularities and well-separated class structure, making them amenable to a wide range of architectures.

The MNIST results are shown in the second column of Fig. 10. For the shallow fully connected architecture (MLP1), persistent entropy decreases monotonically with training loss, indicating progressive simplification of the parameter-space topology. Compared to DIGITS, the decay occurs

over a broader loss range and is accompanied by increased variability at intermediate loss values, reflecting the higher intrinsic complexity of the dataset.

Increasing network depth enhances the stability of the topological signal. The MLP2 row of Fig. 10 shows a smoother decay of persistent entropy and reduced variability across realizations, particularly in the low-loss regime. The strongest stabilization is observed for the convolutional architecture: the CNN row exhibits a pronounced monotone decay together with a marked collapse of variability, indicating rapid convergence of persistence diagrams toward a low-complexity limiting structure.

Neural networks: Fashion-MNIST We then consider the Fashion-MNIST dataset, which represents an intermediate-to-high complexity classification task between MNIST and CIFAR-10. Although it shares the same input dimensionality as MNIST, Fashion-MNIST exhibits substantially higher intra-class variability and weaker low-level statistical regularities.

We analyzed two multilayer perceptron architectures (MLP1 and MLP2) and a convolutional neural network (CNN), each trained on Fashion-MNIST over $R = 5$ independent realizations. Persistent entropy $\text{PE}(H_1)$ was computed from weight-based embeddings as a function of training loss.

The Fashion-MNIST results are summarized in the third column of Fig. 10. For the shallow fully connected architecture (MLP1), persistent entropy decreases monotonically with training loss, indicating progressive topological simplification. However, the decay is slower and accompanied by broader confidence intervals than in the MNIST case, reflecting increased variability across realizations.

Increasing network depth partially compensates for this increased complexity. As shown by the MLP2 row of Fig. 10, the deeper architecture exhibits a smoother decay of persistent entropy and reduced variability, especially in the low-loss regime. A qualitatively stronger stabilization is observed for the convolutional architecture: in the CNN row, persistent entropy decreases systematically with training loss and exhibits substantially narrower confidence intervals, indicating robust convergence toward a low-complexity limiting topology induced by architectural inductive bias.

Neural networks: CIFAR-10 We finally focus on the CIFAR-10 dataset, which constitutes the most complex learning task considered in this study due to its higher input dimensionality, color structure, and nontrivial spatial correlations. This setting provides a stringent test of the topological criterion and highlights the role of inductive bias in enabling convergence toward a stable limiting topology.

The CIFAR-10 results are shown in the rightmost column of Fig. 10. For the shallow fully connected architecture (MLP1), persistent entropy does not exhibit a monotone dependence on training loss and displays wide variability across realizations. After an initial decrease, $\text{PE}(H_1)$ increases again at lower loss values, indicating that different runs explore topologically inequivalent regions of parameter space and that no coherent limiting persistence diagram exists.

Increasing network depth alone does not resolve this issue. As shown in the MLP2 row of Fig. 10, variability across realizations remains large, particularly in the low-loss regime, indicating that depth without appropriate architectural constraints is insufficient to stabilize the geometry induced by learning on CIFAR-10.

A qualitatively different behavior emerges for the convolutional architecture. In the CNN row of Fig. 10, persistent entropy decreases systematically with training loss and exhibits a marked reduction in variability across realizations. This behavior indicates convergence toward a stable

limiting topology and demonstrates that strong architectural inductive bias is essential for satisfying the assumptions of Theorem 1 in this high-complexity setting.

5.4.3 Relation to the general theorem.

The machine learning experiments provide a unified numerical realization of the probabilistic framework underlying Theorem 1 in a high-dimensional, non-physical setting. In this context, neural network training defines, for each dataset–architecture pair and training stage, a random persistence diagram obtained by applying Vietoris–Rips persistent homology to metric embeddings of network parameters. The randomness arises from weight initialization and stochastic optimization, while the training loss \mathcal{L} acts as an effective control parameter governing the distribution of persistence diagrams.

Across all datasets and architectures considered, the behavior of persistent entropy is directly linked to the existence of a limiting persistence diagram in the sense of convergence in probability. For low-complexity tasks such as DIGITS, persistence diagrams converge robustly across architectures as \mathcal{L} decreases, and persistent entropy exhibits a monotone decay with rapid stabilization and collapse of variability across realizations. For intermediate-complexity datasets such as MNIST and Fashion-MNIST, convergence still occurs but with slower rates and increased residual variability, and its robustness depends increasingly on architectural depth and inductive bias. In these regimes, deeper architectures and convolutional structure accelerate and stabilize convergence of the associated persistence diagrams.

For the highest-complexity task considered, CIFAR-10, convergence in probability of persistence diagrams is observed only when strong architectural constraints are present. Fully connected architectures fail to exhibit stabilization of persistent entropy, indicating the absence of a coherent limiting topological structure, whereas convolutional architectures restore monotone decay and variance collapse. This architectural dependence highlights the necessity of inductive bias for satisfying the assumptions of Theorem 1 in complex learning settings.

From the perspective of Theorem 1, these results demonstrate that persistent-entropy phase transitions arise precisely when training dynamics induce a qualitative change in the limiting topological structure, characterized by the disappearance of macroscopic H_1 features and the concentration of persistence diagrams around a low-complexity configuration. Conversely, when no such limiting structure exists, persistent entropy fails to stabilize, in agreement with the violation of the theorem’s hypotheses. Taken together, the machine learning experiments show that the theorem applies beyond physical systems and equilibrium settings, and that persistent entropy provides a robust detector of emergent geometric organization driven by learning dynamics in fully data-driven models.

6 Conclusions

We established a model-independent theoretical criterion showing that persistent entropy detects phase transitions whenever the transition induces a qualitative change in the limiting persistence diagrams at macroscopic scales. In a probabilistic setting where persistence diagrams $D_N(\lambda)$ are random objects, we proved that if diagrams converge in probability to distinct deterministic limits on either side of a critical parameter λ_c and if one phase contains at least one bar with lifetime bounded away from zero while the other contains only vanishingly short bars, then persistent entropy separates the phases by an asymptotically non-vanishing gap. This identifies a precise barcode-level mechanism underlying the widespread empirical use of persistent entropy: PE acts as a detector of the creation or destruction of topological mass at macroscopic lifetimes.

To connect the asymptotic theorem to practical finite-time simulations, we introduced a dynamical operationalization based on topological stabilization. For each control parameter λ , we defined a topological transition time $t_*(\lambda)$ as the first time at which a chosen topological statistic becomes stable on a sliding window, and used the empirical probability $p(\lambda) = \Pr(t_*(\lambda) \leq T_{\max})$ to estimate critical parameters. This approach bridges the limiting-diagram viewpoint of the theorem with the finite-horizon accessibility of ordered states in dynamical systems.

The numerical experiments support the theoretical picture in three complementary settings. In the Kuramoto model, increasing coupling induces synchronization accompanied by a sharp drop and stabilization of persistent entropy, consistent with convergence toward a near-trivial limiting diagram. In the Vicsek model, decreasing noise leads to flocking together with stabilization of persistent entropy and contraction of barcodes, while higher noise prevents convergence within the observation horizon, captured probabilistically by the decay of $p(\eta)$. Finally, in neural network training dynamics, we treated training loss as an effective control parameter and computed persistent entropy from weight-based embeddings across datasets of increasing complexity (DIGITS, MNIST, Fashion-MNIST, CIFAR-10) and architectures (MLP1, MLP2, CNN). The resulting grid comparison shows that persistent entropy exhibits monotone decay and variance collapse precisely when training induces a stable limiting geometry—robustly for low-complexity tasks, and only under appropriate inductive bias for high-complexity tasks such as CIFAR-10—while failing to stabilize when the underlying convergence assumptions are not met.

Taken together, these results clarify both the power and the limitations of persistent entropy as a phase-transition detector: PE is guaranteed to work under explicit convergence and macroscopic-feature separation conditions, and its failures are informative indicators that the limiting-diagram hypotheses are violated. Promising directions for future work include sharpening continuity assumptions for PE under common filtrations (e.g., via principled lifetime truncation), extending the framework to richer diagram summaries beyond entropy, and developing statistical tests for diagram convergence and macroscopic feature separation from finite samples and finite system sizes.

References

- [1] Topological data analysis (TDA) as a framework for understanding deep learning behavior. IEEE, 2024.
- [2] Jens Agerberg, Andrea Guidolin, Andrea Martinelli, and Indika Rajapakse. Certifying robustness via topological representations. *arXiv preprint arXiv:2501.10876*, Jan 2025.
- [3] Nieves Atienza, Rocio Gonzalez-Diaz, and Matteo Rucco. On the stability of persistent entropy and new summary functions for topological data analysis. *Pattern Recognition*, 107:107509, 2020. GAP3: CRITICAL - Stability analysis of persistent entropy functional.
- [4] Romie Banerjee, Feng Liu, and Pei Ke. Towards robust perception using topological invariants, 2021.
- [5] Mathieu Bastian, Sébastien Heymann, and Mathieu Jacomy. Gephi: an open source software for exploring and manipulating networks. In *Third international AAAI conference on weblogs and social media*, 2009.
- [6] Jacopo Binchi, Emanuela Merelli, Matteo Rucco, Giovanni Petri, and Francesco Vaccarino. jHoles: A Tool for Understanding Biological Complex Networks via Clique Weight Rank Persistent Homology. *Electronic Notes in Theoretical Computer Science*, 306:5–18, 2014.

- [7] Rickard Brüel-Gabrielsson, Bradley J. Nelson, Anjan Dwaraknath, Primoz Skraba, Leonidas J. Guibas, and Gunnar Carlsson. A topology layer for machine learning. *arXiv preprint arXiv:1905.12200*, May 2019.
- [8] Peter Bubenik. Statistical topological data analysis using persistence landscapes. *Journal of Machine Learning Research*, 16:77–102, 2015. GAP4: FOUNDATIONAL - Persistence landscapes for statistical analysis of random diagrams.
- [9] Gunnar Carlsson. Topology and data. *Bulletin of the American Mathematical Society*, 46(2):255–308, 2009. FOUNDATIONAL - Comprehensive TDA review.
- [10] Frédéric Chazal, Brittany Terese Fasy, Fabrizio Lecci, Bertrand Michel, Alessandro Rinaldo, and Larry Wasserman. Convergence rates for persistence diagram estimation in topological data analysis. *Journal of Machine Learning Research*, 16:3603–3635, 2015. GAP4: FOUNDATIONAL - Convergence rates and statistical inference for persistence diagrams.
- [11] Muyi Chen, Daling Wang, Shi Feng, Yifei Shi, and Yingjie Ge. Topological regularization for representation learning via persistent homology. *Mathematics*, 11(4):1008, Feb 2023.
- [12] Wei Chen. Scaling theory of topological phase transitions. *Journal of Physics: Condensed Matter*, 28(5):055601, 2016. GAP1: First RG framework for topological invariants with universal scaling.
- [13] Harish Chintakunta, Thanos Gentimis, Rocio Gonzalez-Diaz, Maria-Jose Jimenez, and Hamid Krim. An entropy-based persistence barcode. *Pattern Recognition*, 48(2):391–401, 2015.
- [14] David Cohen-Steiner, Herbert Edelsbrunner, and John Harer. Stability of persistence diagrams. *Discrete & Computational Geometry*, 37(1):103–120, 2007. FOUNDATIONAL - Bottleneck stability theorem for persistence diagrams.
- [15] Tianwei Dai et al. Non-hermitian topological phase transitions controlled by nonlinearity. *Nature Physics*, 19:1780–1786, 2023. GAP1: Driven/dissipative systems where band theory fails.
- [16] G. Juan Diaz Ochoa. Observability of complex systems by means of relative distances between homological groups. *Frontiers in Physics*, 8:465982, Dec 2020.
- [17] Juan G. Diaz Ochoa. A unified method for assessing the observability of dynamic complex systems. *bioRxiv*, 2022. GAP3: FOUNDATIONAL - Diaz contribution linking PE to information theory (Phi-S framework).
- [18] Juan G. Diaz Ochoa. System observability and Φ -S complexity. In *Quantitative Approach to Neuromorphology and Brain Connectivity*, pages 65–84. Springer, 2024. GAP3: FOUNDATIONAL - Published version of Phi-S framework.
- [19] Vincent Divol and Théo Lacombe. Understanding the topology and the geometry of the space of persistence diagrams via optimal partial transport. *Journal of Applied and Computational Topology*, 5:1–53, 2021. GAP4: Optimal transport framework for persistence diagram spaces.
- [20] Herbert Edelsbrunner, David Letscher, and Afra Zomorodian. Topological persistence and simplification. *Discrete & Computational Geometry*, 28(4):511–533, 2002. FOUNDATIONAL - Original persistent homology framework.

[21] Lars Q English. Synchronization of oscillators: an ideal introduction to phase transitions. *European journal of physics*, 29(1):143, 2007.

[22] R. González-Albaladejo, A. Carpio, and L. L. Bonilla. Scale-free chaos in the confined Vicsek flocking model. *Physical Review E*, 107(1):014209, 2023. GAP4: CRITICAL - Finite-size scaling with TDA for Vicsek critical windows.

[23] Yu He, Shiqiang Xia, Dimitris G. Angelakis, Daohong Song, and Zhigang Chen. Persistent homology analysis of a generalized Aubry-André-Harper model. *Physical Review B*, 106(5):054210, 2022. GAP2: Phase-to-persistence mapping with finite-size analysis.

[24] Markus Heyl and Jan Carl Budich. Dynamical topological quantum phase transitions for mixed states. *Physical Review B*, 96(18):180304, 2017. GAP1: Dynamical quantum phase transitions and nonequilibrium topology.

[25] Mohsin Iqbal and Norbert Schuch. Entanglement order parameters and critical behavior for topological phase transitions and beyond. *arXiv preprint arXiv:2011.04595*, 2020. GAP1: Universal critical exponents via tensor networks for topological transitions.

[26] Kazuha Itabashi, Quoc Hoan Tran, and Yoshihiko Hasegawa. Evaluating the phase dynamics of coupled oscillators via time-variant topological features. *Physical Review E*, 103(3):032207, 2021. GAP2: Time-variant topological features for oscillator dynamics.

[27] Kwangho Kim, Jisu Kim, Manzil Zaheer, Joon Kim, Frédéric Chazal, and Larry Wasserman. PLLay: Efficient topological layer based on persistent landscapes. In *Advances in Neural Information Processing Systems*, volume 33, pages 15965–15977, Feb 2020.

[28] Ranjith R. Kumar, Y. R. Kartik, and Sujit Sarkar. Topological phase transition between non-high symmetry critical phases and curvature function renormalization group. *New Journal of Physics*, 25:083010, 2023. GAP1: Extends curvature-function RG to non-symmetric cases, multicritical points.

[29] Emanuela Merelli, Matteo Rucco, Peter Sloot, and Luca Tesei. Topology driven modeling: the IS metaphor. *Natural Computing*, 14(3):421–430, 2015. GAP3: Early conceptual framework for persistent entropy in immune systems.

[30] Yuriy Mileyko, Sayan Mukherjee, and John Harer. Probability measures on the space of persistence diagrams. *Inverse Problems*, 27(12):124007, 2011. GAP4: FOUNDATIONAL - Probabilistic framework for persistence diagrams as random objects.

[31] Edward Ott and Thomas M. Antonsen. Low dimensional behavior of large systems of globally coupled oscillators. *Chaos: An Interdisciplinary Journal of Nonlinear Science*, 18(3):037113, 2008. FOUNDATIONAL - Ott-Antonsen ansatz for Kuramoto model.

[32] Murali Krishna Pasupuleti. *AI in topological data analysis: Understanding high-dimensional data structures*. Nov 2024.

[33] Marco Piangerelli, Matteo Rucco, Luca Tesei, and Emanuela Merelli. Topological classifier for detecting the emergence of epileptic seizures. *BMC Research Notes*, 11(1):368, 2018. GAP2: Applied dynamical phase-like transition detection with persistent entropy.

[34] Matteo Rucco, Filippo Castiglione, Emanuela Merelli, and Marco Pettini. Characterisation of the idiotypic immune network through persistent entropy. In *Proceedings of ECCS 2014*, Springer Proceedings in Complexity, pages 117–128. Springer, 2016. GAP3: FOUNDATIONAL - Original Rucco persistent entropy formulation.

[35] Matteo Rucco, Rocio Gonzalez-Diaz, Maria-Jose Jimenez, Nieves Atienza, Cristina Cristalli, Enrico Concettoni, Andrea Ferrante, and Emanuela Merelli. A new topological entropy-based approach for measuring similarities among piecewise linear functions. *Signal Processing*, 134:130–138, 2017. GAP3: Early Rucco work on persistent entropy for signal comparison.

[36] S. Rufo, Nei Lopes, Mucio A. Continentino, and M. A. R. Griffith. Multicritical behavior in topological phase transitions. *Physical Review B*, 100(19):195432, 2019. GAP1: Universality classes via edge-mode penetration lengths and Berry connection scaling.

[37] Isac Sahlberg, Alex Westström, Kim Pichler, Björgvin Hjörvarsson, Battulga Munkhbat, Timur Shegai, and Jonas Johansson. Topological phase transitions in glassy quantum matter. *Physical Review Research*, 2(1):013053, 2020. GAP4: Amorphous systems with nonuniversal scaling and sample-to-sample variability.

[38] A. Stolarek and W. Jaworek. Preserving information: How does topological data analysis improve neural network performance? *arXiv preprint arXiv:2411.18410*, Nov 2024.

[39] Bernadette J. Stoltz, Heather A. Harrington, and Mason A. Porter. Persistent homology of time-dependent functional networks constructed from coupled time series. *Chaos: An Interdisciplinary Journal of Nonlinear Science*, 27(4):047410, 2017. GAP2: CRITICAL - Kuramoto time series, filtration-to-synchronization mapping.

[40] Bernadette J Stoltz, Heather A Harrington, and Mason A Porter. Persistent homology of time-dependent functional networks constructed from coupled time series. *Chaos: An Interdisciplinary Journal of Nonlinear Science*, 27(4):047410, 2017.

[41] Steven H. Strogatz. From Kuramoto to Crawford: exploring the onset of synchronization in populations of coupled oscillators. *Physica D: Nonlinear Phenomena*, 143(1-4):1–20, 2000. FOUNDATIONAL - Comprehensive review of Kuramoto model.

[42] John Toner, Yuhai Tu, and Sriram Ramaswamy. Hydrodynamic equations for self-propelled particles: microscopic derivation and stability analysis. *Annals of Physics*, 318(1):170–244, 2005. FOUNDATIONAL - Toner-Tu hydrodynamic theory of flocking.

[43] Chad M. Topaz, Lori Ziegelmeier, and Tom Halverson. Topological data analysis of biological aggregation models. *PLOS ONE*, 10(5):e0126383, 2015. GAP2: CRITICAL - Direct application to Vicsek model, links transitions to persistence structure.

[44] Tamás Vicsek, András Czirók, Eshel Ben-Jacob, Inon Cohen, and Ofer Shochet. Novel type of phase transition in a system of self-driven particles. *Physical Review Letters*, 75(6):1226–1229, 1995. FOUNDATIONAL - Original Vicsek flocking model.

[45] Bohm-Jung Yang, Eun-Gook Moon, Hiroki Isobe, and Naoto Nagaosa. Quantum criticality of topological phase transitions in three-dimensional interacting electronic systems. *Nature Physics*, 10(10):774–778, 2014. GAP1: Interacting topological criticality beyond single-particle band theory.

[46] Álvaro Zabaleta-Ortega, Cristina Masoller, and L. Guzmán-Vargas. Topological data analysis of the synchronization of a network of Rössler chaotic electronic oscillators. *Chaos: An Interdisciplinary Journal of Nonlinear Science*, 33(11):113109, 2023. GAP2: CRITICAL - Persistent entropy tracks coupling-driven synchronization transitions.

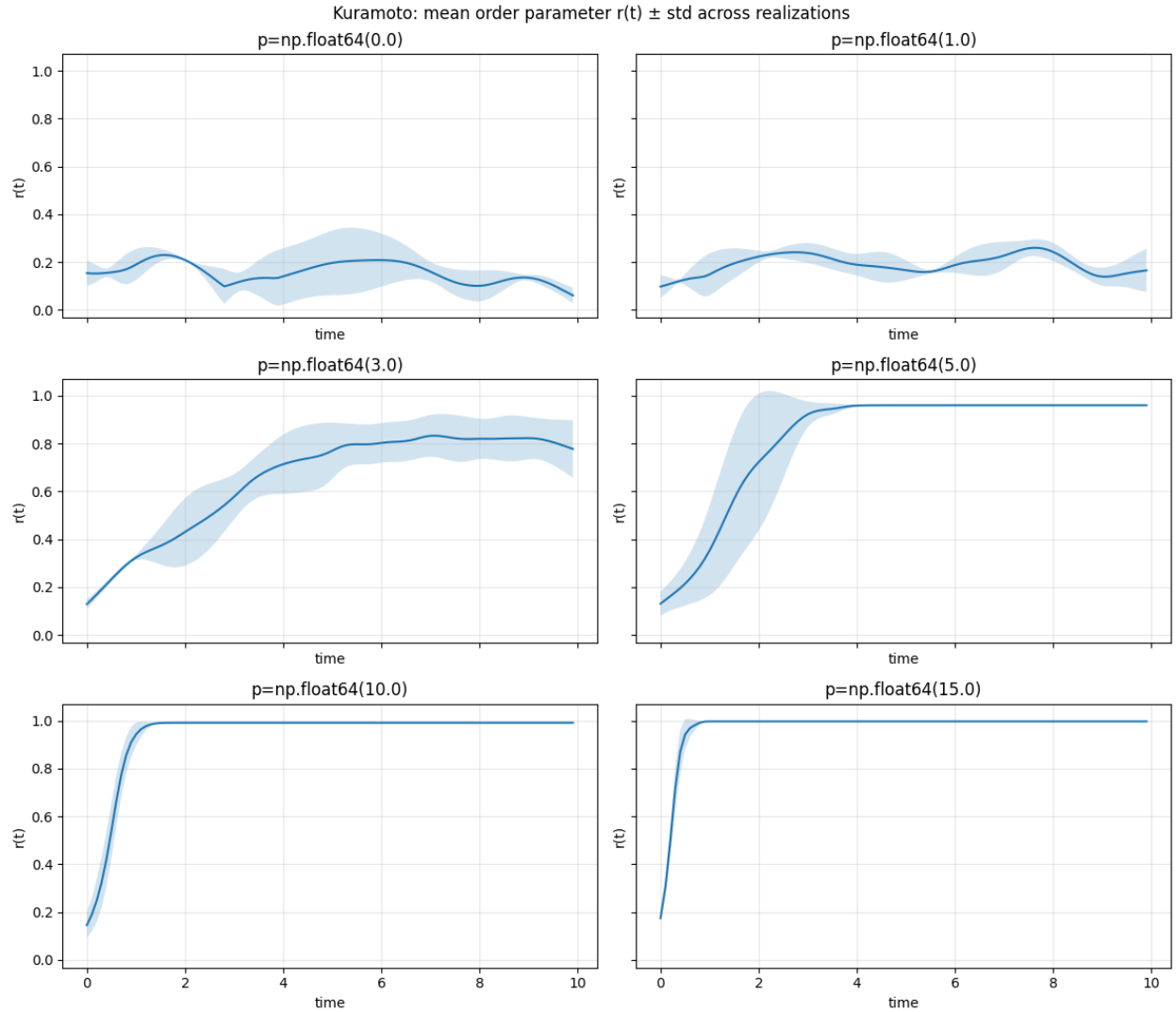


Figure 2: Kuramoto order parameter $r(t)$ for increasing coupling values K . Solid lines represent the mean across realizations, while shaded regions indicate one standard deviation. A sharp transition from incoherent dynamics to full synchronization is observed as K increases.

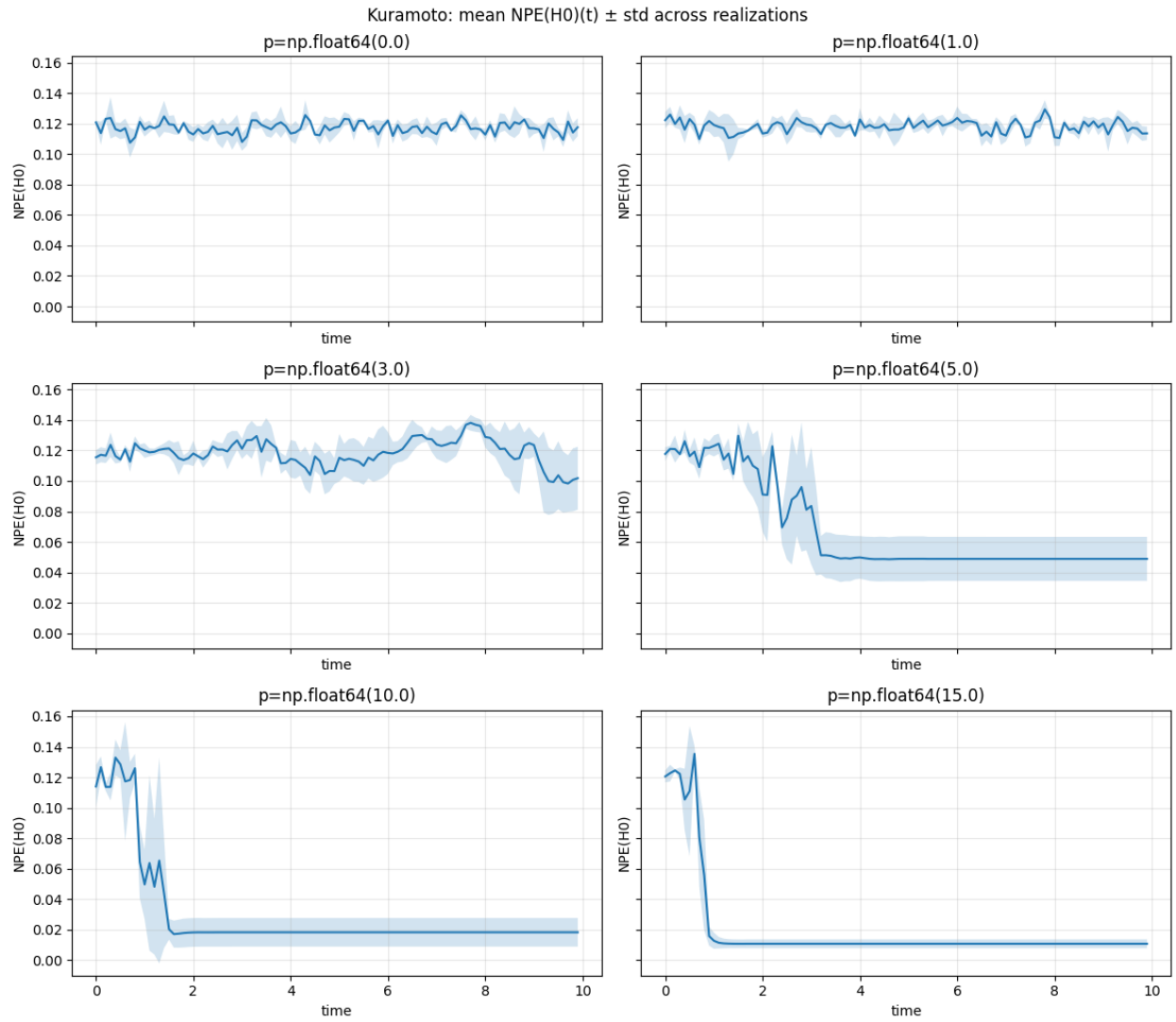


Figure 3: Temporal evolution of the normalized persistent entropy $NPE(H_0)(t)$ for the Kuramoto model across different coupling strengths K . For low coupling, persistent entropy fluctuates around a high value, while for sufficiently large K it rapidly drops and stabilizes, indicating a collapse of topological complexity.

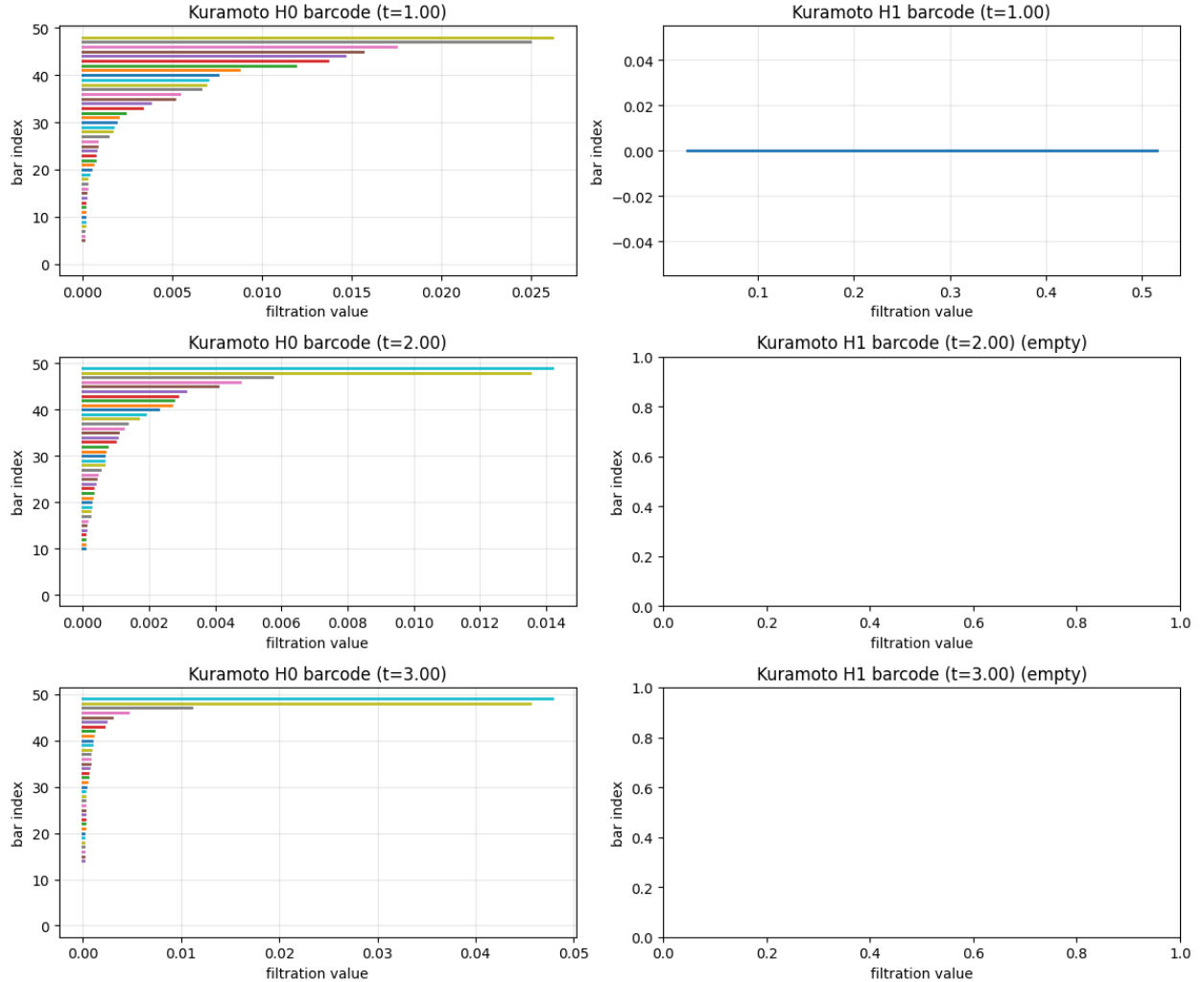


Figure 4: Persistence barcodes for the Kuramoto model at three representative time points ($t = 1.0$, $t = 2.0$, $t = 3.0$) for coupling strength $K = 5$. Left panels show H_0 barcodes, while right panels show H_1 barcodes. The collapse of H_0 bars and the absence of persistent H_1 features indicate convergence toward a fully synchronized configuration.

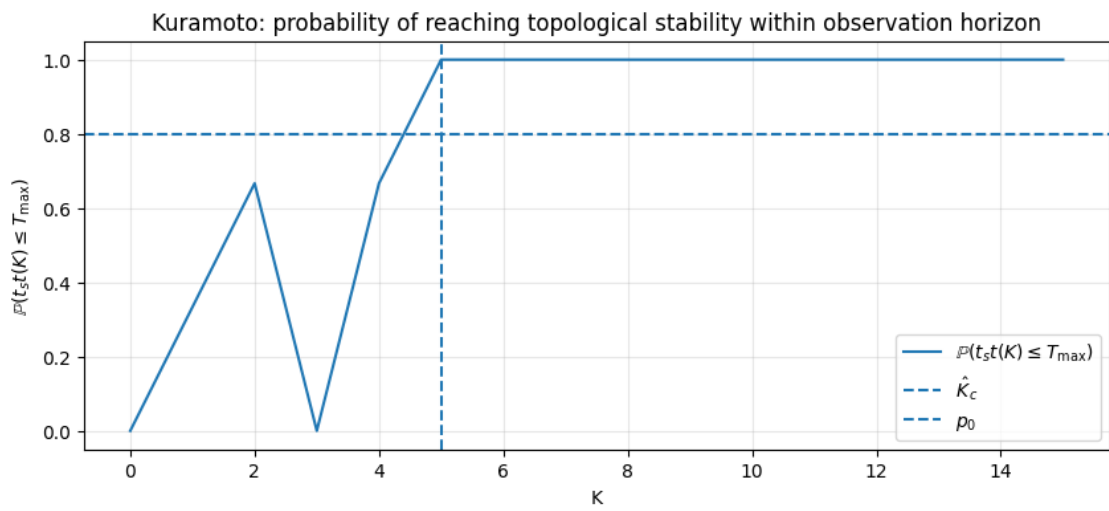


Figure 5: Probability $\mathbb{P}(t_*(K) \leq T_{\max})$ of reaching topological stability within the observation horizon as a function of the coupling strength K . The horizontal dashed line denotes the confidence threshold p_0 , while the vertical dashed line marks the estimated critical coupling \hat{K}_c .

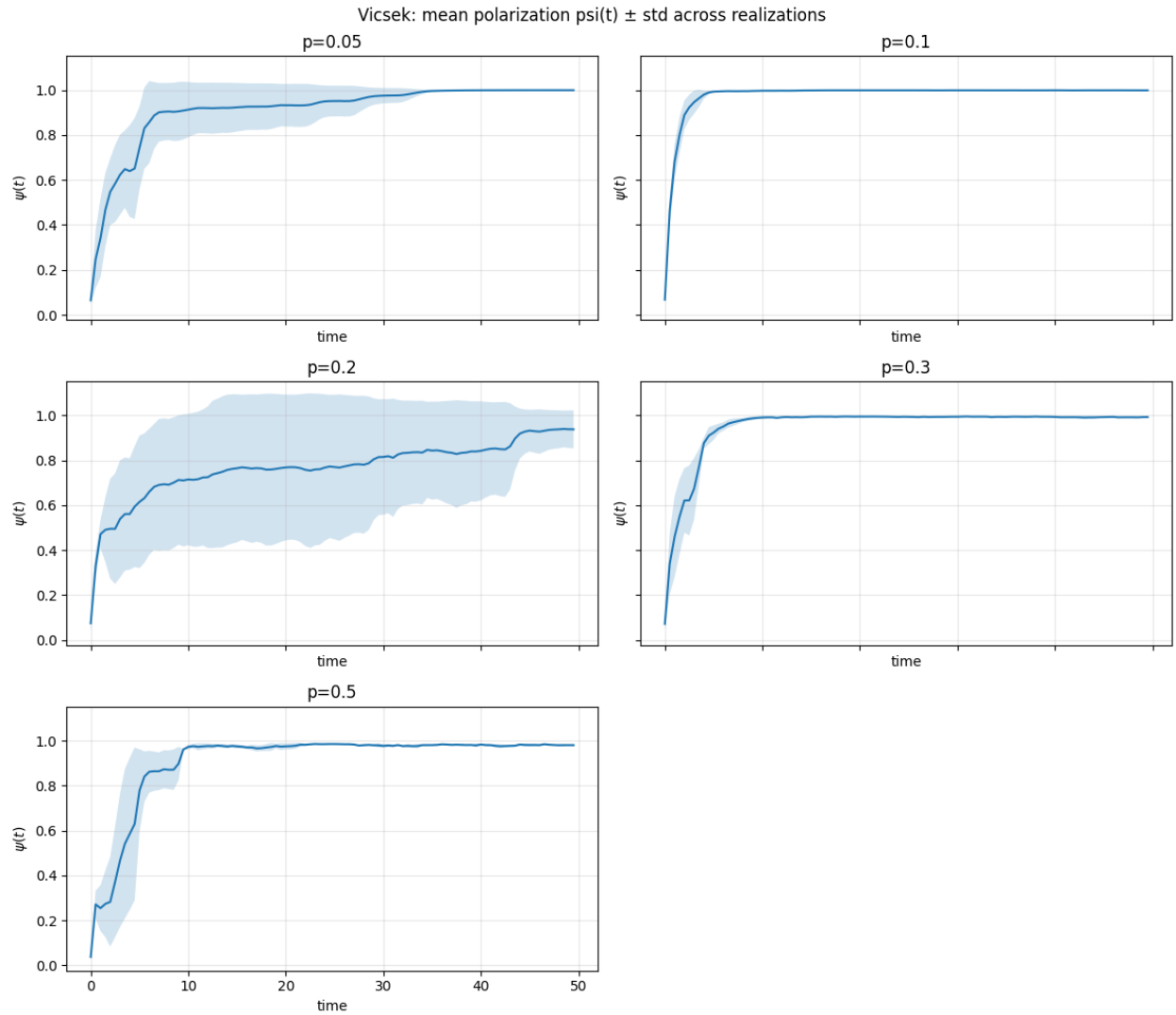


Figure 6: Mean Vicsek polarization $\psi(t)$ with standard deviation across realizations for different noise amplitudes η . Low noise leads to rapid convergence toward $\psi(t) \simeq 1$, while increasing noise delays or suppresses global ordering.

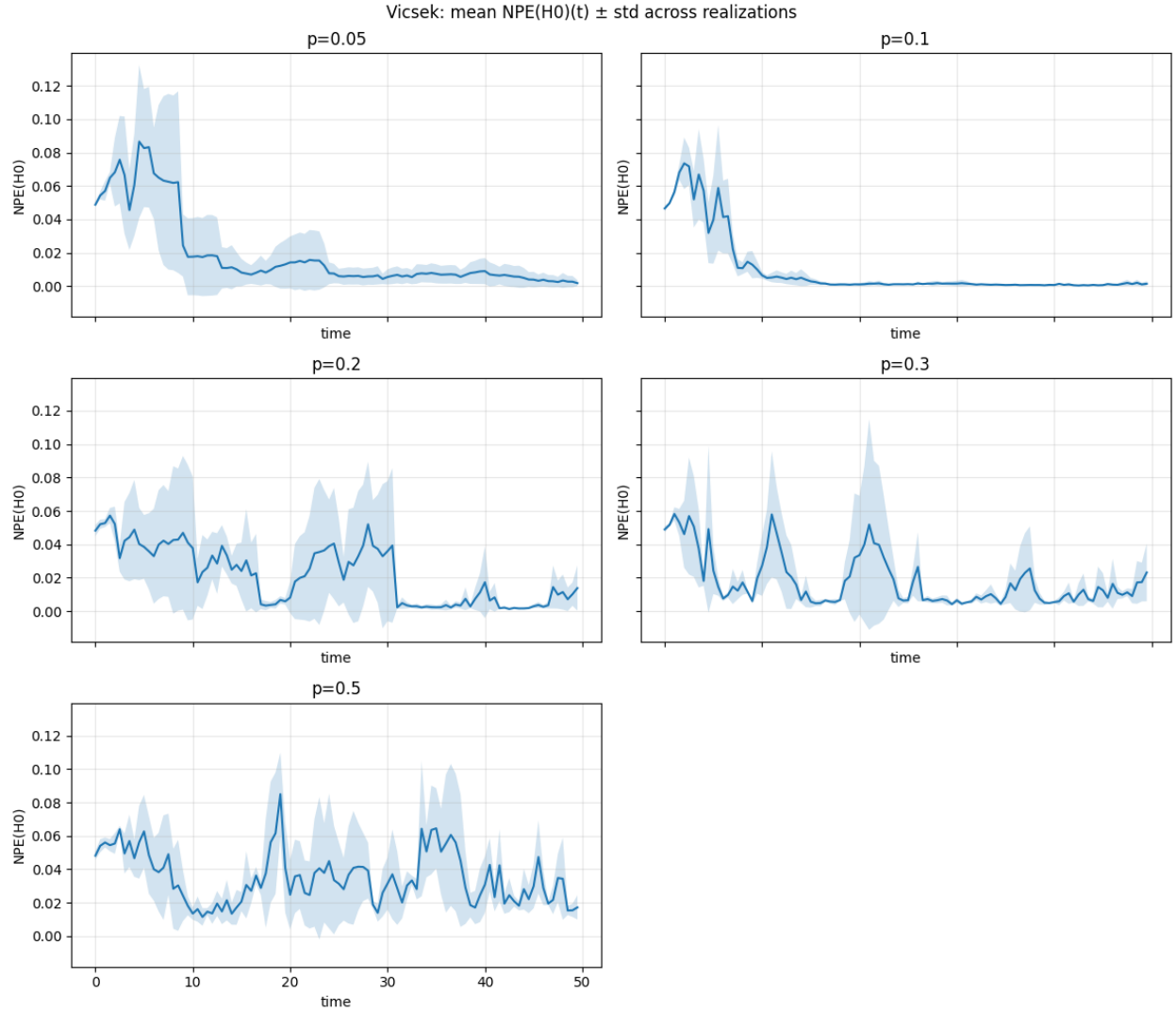


Figure 7: Temporal evolution of the normalized persistent entropy $NPE(H_0)(t)$ for the Vicsek model across increasing noise amplitudes η . Solid lines denote the mean across realizations, while shaded regions indicate one standard deviation. Low-noise regimes exhibit a rapid decay and stabilization of persistent entropy, whereas higher noise levels are associated with sustained fluctuations.

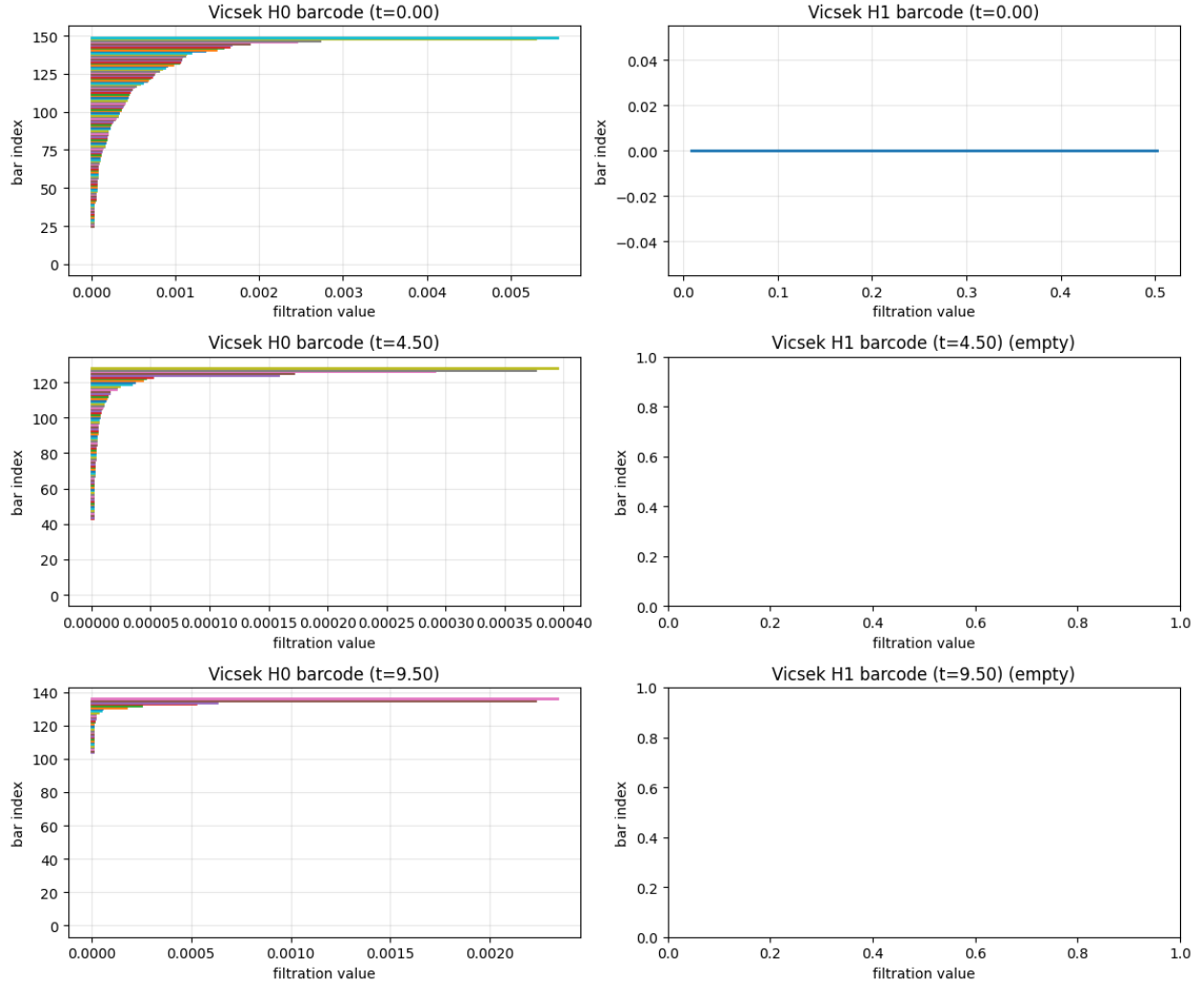


Figure 8: Persistence barcodes for the Vicsek model at three representative times ($t = 0.0$, $t = 4.5$, $t = 9.5$) for noise amplitude $\eta = 0.1$. Left panels show H_0 barcodes, while right panels show H_1 barcodes. The progressive collapse of H_0 bars and the absence of persistent H_1 features indicate convergence toward an ordered flocking configuration.

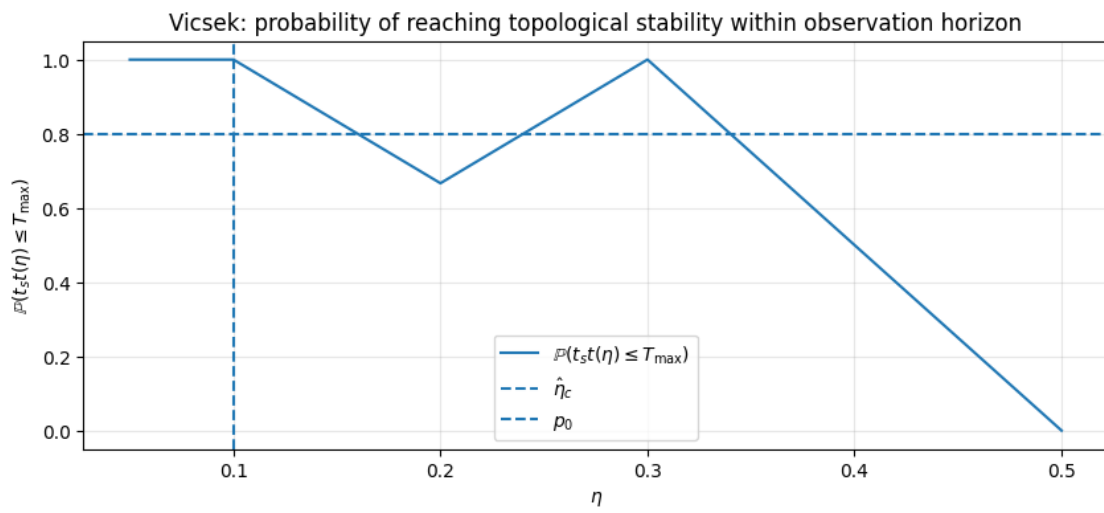


Figure 9: Probability $\mathbb{P}(t_*(\eta) \leq T_{\max})$ of reaching topological stability within the observation horizon as a function of the noise amplitude η . The horizontal dashed line indicates the confidence threshold p_0 , while the vertical dashed line marks the estimated critical noise $\hat{\eta}_c$.

Algorithm 2: Persistent entropy monitoring during neural network training

Input: Dataset $\mathcal{D} = \{(x_i, y_i)\}_{i=1}^n$; architecture \mathcal{A} ; training procedure **Train** (optimizer, epochs T , batch size, etc.); number of runs R ; layer set \mathcal{L} (hidden layers to monitor); embedding mode $\text{mode} \in \{\text{WEIGHTS}, \text{ACTIVATIONS}\}$; PH degree k (typically $k = 1$); filtration type **VR** (Vietoris–Rips); optional truncation threshold $\tau \geq 0$; loss-binning scheme \mathcal{B} .

Output: Histories $\{H^{(r)}\}_{r=1}^R$ with tuples $(t, \mathcal{L}^{(r)}(t), PE_k^{(r)}(t))$; optional binned curves $\overline{PE}_k(\ell)$ with confidence intervals.

for $r = 1$ **to** R **do**

- Initialize network parameters $\theta^{(r)}(0)$ with random seed s_r ;
- Initialize empty history $H^{(r)} \leftarrow []$;
- for** $t = 1$ **to** T **do**

 - // 1) Perform one training epoch / step
 - $\theta^{(r)}(t) \leftarrow \text{Train}(\mathcal{A}, \mathcal{D}, \theta^{(r)}(t-1))$;
 - Compute training loss $\mathcal{L}^{(r)}(t)$;
 - // 2) Build a point cloud from the chosen embedding
 - if** $\text{mode} = \text{WEIGHTS}$ **then**

 - // Neurons as points via incoming weights (and bias if present)
 - Construct point cloud $X^{(r)}(t) = \bigcup_{\ell \in \mathcal{L}} \{w_{j,\ell}^{(r)}(t)\}_{j=1}^{m_\ell}$;

 - else**

 - // Samples as points via hidden activations on a fixed probe set
 - Choose a fixed probe subset $\mathcal{D}_{\text{probe}} \subset \mathcal{D}$;
 - Construct $X^{(r)}(t) = \bigcup_{\ell \in \mathcal{L}} \{a_\ell^{(r)}(x; t) : x \in \mathcal{D}_{\text{probe}}\}$;

 - // 3) Compute distances and persistent homology
 - Compute pairwise distances $d^{(r)}(t)$ on $X^{(r)}(t)$ (e.g., Euclidean);
 - Build Vietoris–Rips filtration $\text{VR}(X^{(r)}(t), d^{(r)}(t))$;
 - Compute persistence diagram $D_k^{(r)}(t)$ in degree k ;
 - // 4) Compute persistent entropy (with optional truncation)
 - Extract lifetimes $\{\ell_i\}$ from $D_k^{(r)}(t)$, where $\ell_i = d_i - b_i$;
 - if** $\tau > 0$ **then**

 - Discard bars with $\ell_i < \tau$;

 - $L \leftarrow \sum_i \ell_i$;
 - if** $L = 0$ **then**

 - $PE_k^{(r)}(t) \leftarrow 0$;

 - else**

 - $p_i \leftarrow \ell_i / L$;
 - $PE_k^{(r)}(t) \leftarrow - \sum_i p_i \log p_i$;

 - Append $(t, \mathcal{L}^{(r)}(t), PE_k^{(r)}(t))$ to $H^{(r)}$;

- // 5) Aggregate across runs using loss as effective control parameter
- if** $\mathcal{B} \neq \emptyset$ **then**

 - Pool all pairs $(\mathcal{L}^{(r)}(t), PE_k^{(r)}(t))$ across r, t ;
 - Partition loss values into bins $\mathcal{B} = \{B_1, \dots, B_M\}$;
 - for** $m = 1$ **to** M **do**

 - Compute mean $\overline{PE}_k(B_m)$ and uncertainty (e.g., 95% CI) over samples in B_m ;

return $\{H^{(r)}\}_{r=1}^R$ and (optionally) binned summaries $\overline{PE}_k(\ell)$;

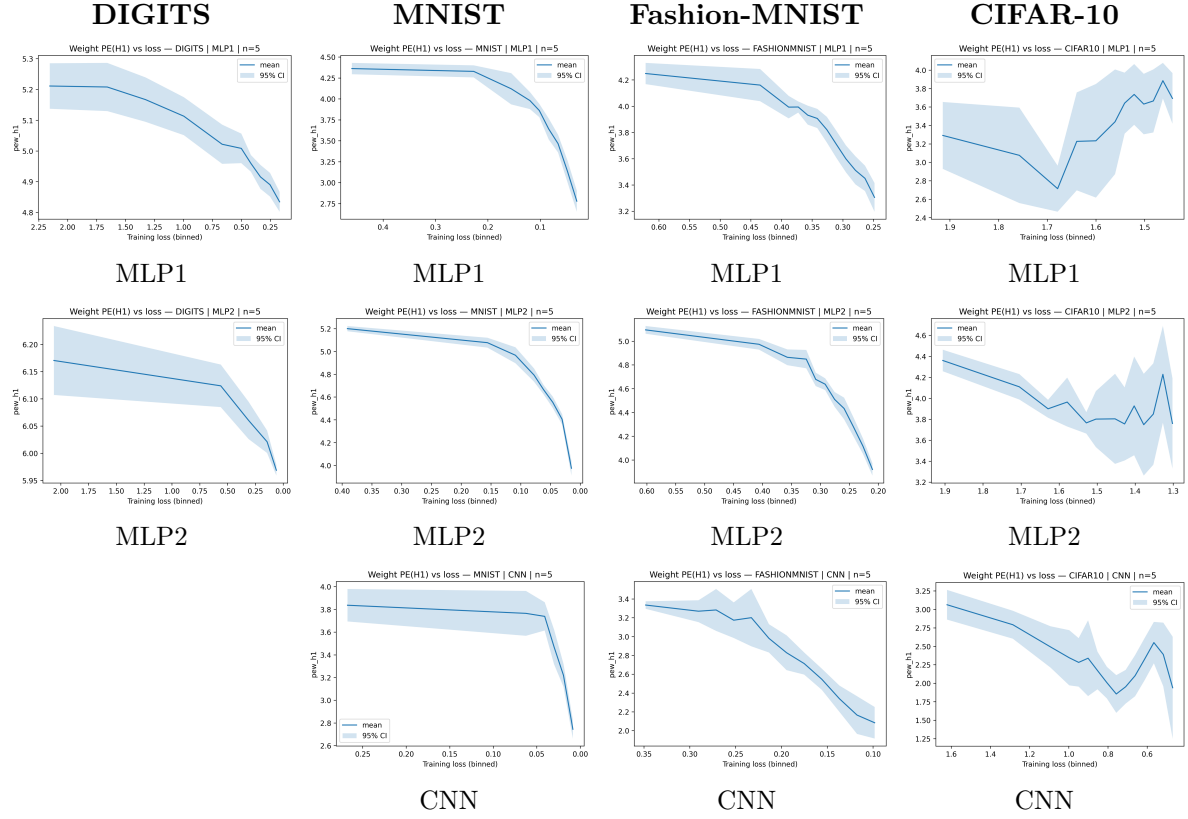


Figure 10: Binned persistent entropy $PE(H_1)$ of weight-based embeddings as a function of training loss across datasets and architectures. Columns correspond to datasets of increasing complexity (DIGITS, MNIST, Fashion-MNIST, CIFAR-10), while rows correspond to network architectures (MLP1, MLP2, CNN). Solid lines denote mean values across $R = 5$ realizations and shaded regions indicate 95% confidence intervals. The emergence of a monotone decay and variance collapse depends jointly on dataset complexity and architectural inductive bias.